Photodegradable glyco-microfibers fabricated by the self-assembly of cellobiose derivatives bearing nitrobenzyl groups

Bioru Okumura[1†], Eriko Yamaguchi[2†], Naoko Komura[2*], Taku Ohtomi[1], Shin-ichiro Kawano[3], Hiroshi Katagiri[4,5], Hiromune Ando[2*], Masato Ikeda[1,2,6,7,8*]

[1] *Department of Life Science and Chemistry, Graduate School of Natural Science and Technology, Gifu University, 1-1 Yanagido, Gifu 501-1193, Japan*

[2] *Institute for Glyco-core Research (iGCORE), Gifu University, 1-1 Yanagido, Gifu 501-1193, Japan*

[3] *Department of Chemistry, Faculty of Science, Nagoya University, Furo-cho, Chikusa-ku, Nagoya 464-8602, Japan*

[4] *Graduate School of Science and Engineering, Yamagata University, 4-3-16 Jonan, Yonezawa, Yamagata 992-8510, Japan*

[5] *Graduate School of Organic Materials Science, Yamagata University, 4-3-16 Jonan, Yonezawa, Yamagata 992-8510, Japan*

[6] *Center for One Medicine Innovative Translational Research (COMIT), Gifu University, 1-1 Yanagido, Gifu 501-1193, Japan*

[7] *United Graduate School of Drug Discovery and Medical Information Sciences, Gifu University, 1-1 Yanagido, Gifu 501-1193, Japan*

[8] *Institute of Nano-Life-Systems, Institutes of Innovation for Future Society, Nagoya University, Furo-cho, Chikusa-ku, Nagoya 464-8603, Japan*

*Correspondence:

N. K.: komura.naoko.a1@f.gifu-u.ac.jp, orcid.org/0000-0002-8104-750X

H. A.: ando.hiromune.i0@f.gifu-u.ac.jp, orcid.org/0000-0002-0551-0830

M. I.: ikeda.masato.n3@f.gifu-u.ac.jp, orcid.org/0000-0003-4097-8292

[†]These authors contributed equally: Bioru Okumura and Eriko Yamaguchi

Graphical Abstract

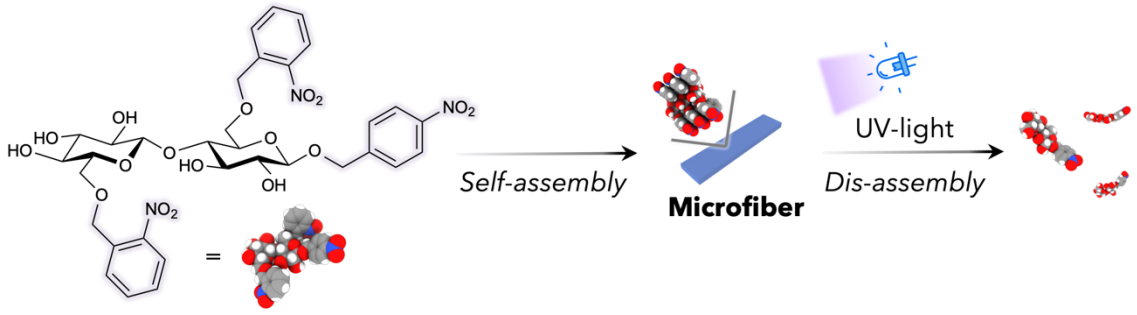

Abstract

Stimuli-responsive materials constructed via the self-assembly of small biomolecules are attracting increasing attention because of their biocompatibility, sustainability, and variety of (bio)applications. Nevertheless, the research on oligosaccharide-based molecular designs for such stimuli-responsive materials (or stimuli-responsive glyco-materials) is limited, partly due to the intrinsic structural diversity of oligosaccharides and the difficulty associated with their selective chemical syntheses. Herein, we report the construction of photodegradable glyco-microfibers by the self-assembly of cellobiose derivatives bearing nitrobenzyl groups. The atomic-scale, self-assembled architecture of the photodegradable glyco-microfibers is unveiled and compared with those of pristine cellobiose and cellulose polymorphs in previous reports.

Stimuli-responsive nano- and micromaterials, constructed through the molecular self-assembly of small biomolecules, such as peptides, nucleic acids, and saccharides, are attracting considerable attention because of their biocompatibility, sustainability, and variety of (bio)applications [1-3]. In particular, short peptides (including di- and tripeptides) have recently become pledged scaffolds that can be equipped with stimuli-responsive functions and exploited to construct a variety of stimuli-responsive supramolecular materials [4-6]. Conversely, the research on oligosaccharide-based molecular design methods for such stimuli-responsive materials (hereinafter referred to as stimuli-responsive glyco-materials) is limited. This is partly due to the intrinsic structural diversity of oligosaccharides (e.g., there are theoretically 11 possible chemical structures for the simple disaccharides of D-glucose) and the difficulty associated with selectively synthesizing desired molecular scaffolds and/or purifying the corresponding available natural products. However, from a different perspective, such chemical diversity may offer a distinct opportunity to construct less-explored molecular libraries for the fabrication of supramolecular architectures.

Recently, Delbianco, Seeberger and coworkers fabricated supramolecular architectures in aqueous media from a disaccharide (i.e., gentiobiose) bearing simple phenyl groups at discrete positions [7,8]. However, cellobiose or cello-oligosaccharides, in which glucose units are linked by β-1,4-linkage, bearing aromatic groups have received little attention in the papers despite their potential to form well-ordered, self-assembled structures under aqueous conditions, as well as the abundance of cellulose-based supramolecular architectures and materials in nature [9,10]. Notably, the enzymatic synthesis of cello-oligosaccharides and the production of the corresponding nanomaterials have been actively explored. For instance, Serizawa and coworkers carried out inspiring studies on the enzymatic synthesis of cello-oligosaccharides facilitated by an enzyme, namely cellodextrin phosphorylase, and the simultaneous construction of nanoribbons through their self-assembly [11,12]. Very recently, Ogawa, Delbianco and coworkers reported the solid-phase synthesis of

cello-oligosaccharides consisting of D- and L-glucose, which required artificial chemical (solid-phase) synthesis instead of enzymatic synthesis because of the unnatural substrate (L-glucose) and the formation of controlled chiral nanostructures [13]. Nonetheless, the research area focusing on molecular design approaches for self-assembly molecules based on oligosaccharide scaffolds that gives rise to stimuli-responsive glyco-materials is still in its infancy.

Herein, we present a molecular design method for the construction of photo-responsive glyco-materials, particularly photodegradable glyco-microfibers, which prioritizes cellobiose as the molecular scaffold. To equip the supramolecular architectures consisting of self-assembling molecules with stimuli-responsive functions, a modular molecular design has been demonstrated to be a promising approach. Further, rational molecular design methods for equipping peptides and nucleic acids with photo- and redox-responsiveness have been explored by several research groups, including ours [14-16]. Nevertheless, the research area focusing on equipping self-assembled supramolecular architectures of oligosaccharide derivatives with such stimuli-responsiveness, affording stimuli-responsive glyco-materials, is largely unexplored. Meanwhile, this study provides a unique opportunity to explore the various (bio)applications of newly constructed photo-responsive glyco-microfibers. Furthermore, the atomic-scale supramolecular architectures of the self-assembled cellobiose derivatives are unveiled and compared with those of pristine cellobiose and cellulose polymorphs. Such structural elucidation will offer valuable insights into the rational molecular design of glyco-materials based on the cellobiose scaffold.

Results and discussion

Molecular design and synthesis of cellobiose(oNB$_2$)-pNB. We designed and synthesized cellobiose derivatives bearing two *o*-nitrobenzyl (oNB) groups at the C6 positions to confer photo-responsiveness on the self-assembled glyco-materials, as displayed in **Fig. 1a**. Previous studies on the aqueous self-assembly of amino acid or peptide derivatives [17-19] have suggested that the *p*-nitrobenzyl (pNB) group introduced at the C1 atom (the reducing end of cellobiose) in this study could promote self-assembly under aqueous conditions. This is probably due to the stronger π–π interactions expected for electron-deficient aromatic groups capable of adopting offset (parallel displaced) stacking [20,21]. Cellobiose(oNB$_2$)-pNB was synthesized according to the concise scheme displayed in **Fig. 1b** (see also, Supplementary **Scheme S1**). In brief, 6-*O*-oNB-modified D-glucose donor **1** and 6-*O*-oNB-modified D-glucose acceptor **2** were glycosylated in the presence of trimethylsilyl trifluoromethanesulfonate (TMSOTf) to afford the corresponding cellobiose (**3**) in 64% yield. Subsequently, cellobiose **3** was glycosylated with pNB alcohol under the NIS(*N*-iodosuccinimide)–TfOH(trifluoromethanesulfonic acid) promoter system, affording pNB-glycosylated cellobiose (**4**) in 83% yield. Finally, the deprotection of **4** over two steps afforded cellobiose(oNB$_2$)-pNB. The newly synthesized

cellobiose(oNB$_2$)-pNB was unambiguously characterized by ^{1}H and ^{13}C nuclear magnetic resonance (NMR) spectroscopy and high-resolution mass spectrometry measurements (see Supplementary Information for details). Notably, the present synthetic scheme can be employed for the systematic introduction of a variety of functional groups, including pNB in this study, to the reducing end of the cellobiose(oNB$_2$) scaffold (at glycosidation steps from **3** to **4**, **Fig. 1b**), without the loss of potential photo-responsiveness.

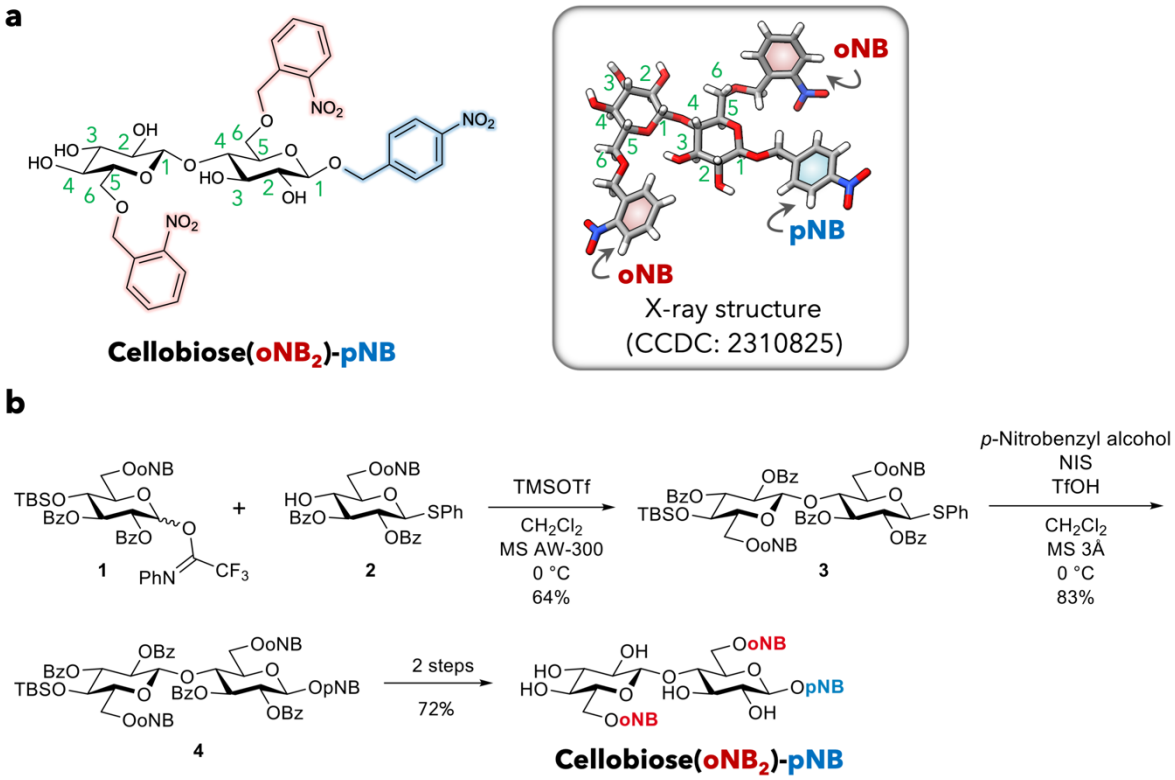

Fig. 1 Molecular design and synthesis of cellobiose(oNB$_2$)-pNB. a Chemical structure of cellobiose(oNB$_2$)-pNB [X-ray structure (CCDC: 2310825) of cellobiose(oNB$_2$)-pNB is also shown, *vide infra* (**Figs. 4**, **5**)]. **b** Synthesis scheme of cellobiose(oNB$_2$)-pNB from glucose derivatives (**1** and **2**) (see Supplementary Information for the experimental procedures and Supplementary **Scheme S1** for the complete synthesis scheme).

Properties of aqueous self-assembled cellobiose(oNB$_2$)-pNB. To control the self-assembly structural morphology of cellobiose(oNB$_2$)-pNB under aqueous conditions and investigate the effect of the concentration and cooling rate on its morphology, cellobiose(oNB$_2$)-pNB at different concentrations [0.05, 0.10, and 0.20 wt% in 100 mM HEPES (4-(2-hydroxyethyl)-1-piperazineethanesulfonic acid)-NaOH (pH 7.4) containing dimethyl sulfoxide (DMSO), as typical aqueous solutions] was subjected to thermal treatment. The treatment procedure was as follows: heating at 95 °C for 5 min, followed by cooling at 5.0, 20, and 30 °C/min using a conventional

thermal cycler, according to the protocol depicted in **Fig. 2a**. Subsequently, the morphology of the self-assembled structures of cellobiose(oNB_2)-pNB in the suspensions obtained after thermal treatment was determined by optical microscopy (OM) and polarized optical microscopy (POM, under cross-polarizers). The morphology was dependent on not only the concentrations but also the cooling rate in the preparation of the aqueous suspension, as summarized in **Fig. 2b**. In brief, at low concentrations and high cooling rates, such as 0.05 wt% (0.67 mM) and 30 °C/min, microspheres were found (**Fig. 2c)**, the average diameter of which was 2.04 ± 0.97 μm (n = 70). In contrast, at high concentrations and low cooling rates, such as 0.10 wt% (1.3 mM) and 5.0 °C/min, long (over several hundred μm) microfibers were observed, as shown in **Fig. 2c_i**. In addition, from the POM images shown in **Fig. 2c_ii**, the microfibers exhibit stronger birefringence than the microspheres, suggesting that the cellobiose(oNB_2)-pNB molecules in the microfibers have crystalline and/or ordered structures. These results motivated us to investigate the time-dependent morphological transformation of the microspheres, which would be considered as molecule-rich condensates [22,23]. As anticipated, the emergence and growth of long microfibers, i.e., the structural transformation from microspheres to microfibers, was observed (**Fig. 2c**, from "**iii** & **iv**" to "**v** & **vi**"). As shown in **Fig. 2c_v**, the length of the microfibers increased and reached more than 100 μm after 6 h. To obtain further insight into the structural transformation, the influence of the Hofmeister effect [24,25] was examined. Without using the buffering component (i.e., HEPES), microfibers were formed directly after cooling (Supplementary **Fig. S1**). Conversely, the presence of SCN^-, as a chaotropic anion, resulted in the transformation of the initially obtained microspheres into microfibers, which is comparable to the result for the aqueous HEPES buffer described above. In contrast, microfibers were directly formed in the presence of Cl^-, as a representative kosmotropic anion (Supplementary **Fig. S2**). These results suggest that the dehydration of the self-assembled structures plays an important role in their transformation from microspheres into microfibers. Collectively, the proposed mechanism of the thermally induced aqueous self-assembly of cellobiose(oNB_2)-pNB to form microfibers is depicted in **Fig. 2d.** A similar structural transformation from spherical to fibrous architecture has been reported for peptide- and protein-based self-assemblies [22,23]. According to the reports, Ostwald ripening and nucleation-induced crystallization in liquid–liquid phase separated state could play important roles in the formation of supramolecular fibrous architectures [26].

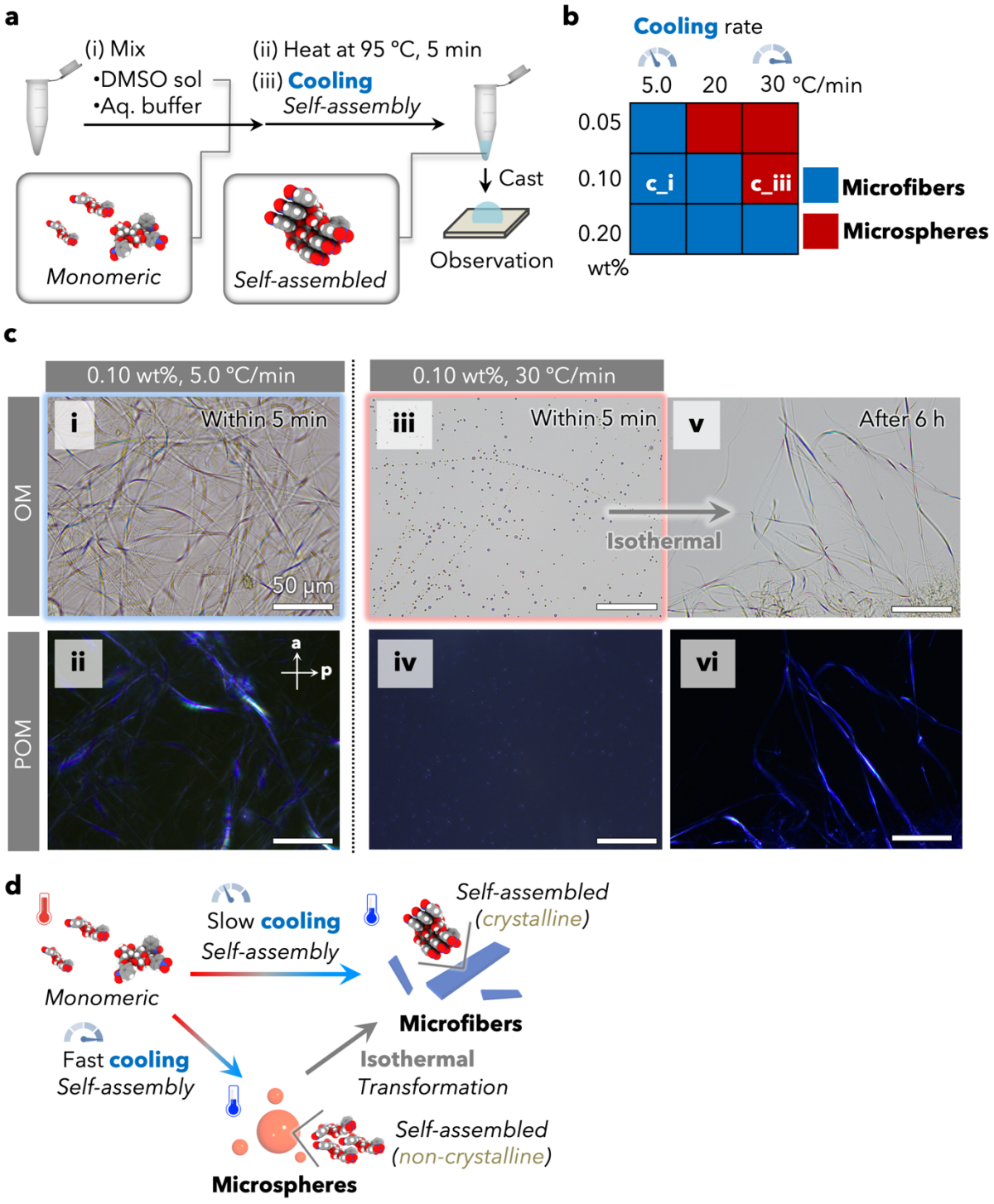

Fig. 2 Thermally induced aqueous self-assembly of cellobiose(oNB$_2$)-pNB. a Representative procedure for the preparation of the self-assembled structures of cellobiose(oNB$_2$)-pNB through a thermal process under aqueous conditions. **b** Morphology of cellobiose(oNB$_2$)-pNB observed within 5 min after cooling to 25 °C at different rates, depending on its concentration. **c** Representative optical microscopic (OM, panels **i**, **iii**, **v**) and polarized optical microscopic (POM, under cross-polarizers, panels **ii**, **iv**, **vi**) images of the self-assembled

structures of cellobiose(oNB_2)-pNB. *Conditions*: [cellobiose(oNB_2)-pNB] = 0.05, 0.10, and 0.20 wt%; 100 mM HEPES-NaOH (pH 7.4) containing 1, 2, and 4 vol% DMSO, rt. See Supplementary **Fig. S1** for more details. **d** Schematic representation of cooling rate dependent formation of microspheres and microfibers through aqueous self-assembly and the isothermal transformation from microspheres into microfibers.

Structural elucidation of the glyco-microfibers consisting of cellobiose(oNB_2)-pNB. To obtain further insight into the structure of the cellobiose(oNB_2)-pNB microfibers at the nanoscale, a series of microscopic analyses [transmission and scanning electron microscopy (TEM, SEM) and atomic force microscopy (AFM), **Fig. 3**] were performed. As shown in **Fig. 3a**, ribbon-like nanostructures were observed in the TEM images. Moreover, the magnified TEM image (**Fig. 3a_ii**) revealed the presence of stripes along the long axis of the ribbon-like nanostructures, and relatively thin fibers were concurrently observed with the ribbon-like nanostructures in the low-magnification TEM image (**Fig. 3a_i**). These indicate that the microfibers observed in the OM images (**Fig. 2c**) can be attributed to the flat ribbon-like nanostructures assembled from thin nanofibrils. A similar morphology was observed in the SEM images (**Fig. 3b**) and AFM height images (**Fig. 3c_i**), which further supports the view that the nanofibril structures can be assembled into ribbon-like nanostructures. In addition, the height of the nanofibrils was evaluated to be approximately 2 nm from the AFM cross-sectional profile (**Fig. 3c_ii**), which is almost consistent with the atomic-scale structural analysis result based on the X-ray structure (*vide infra*).

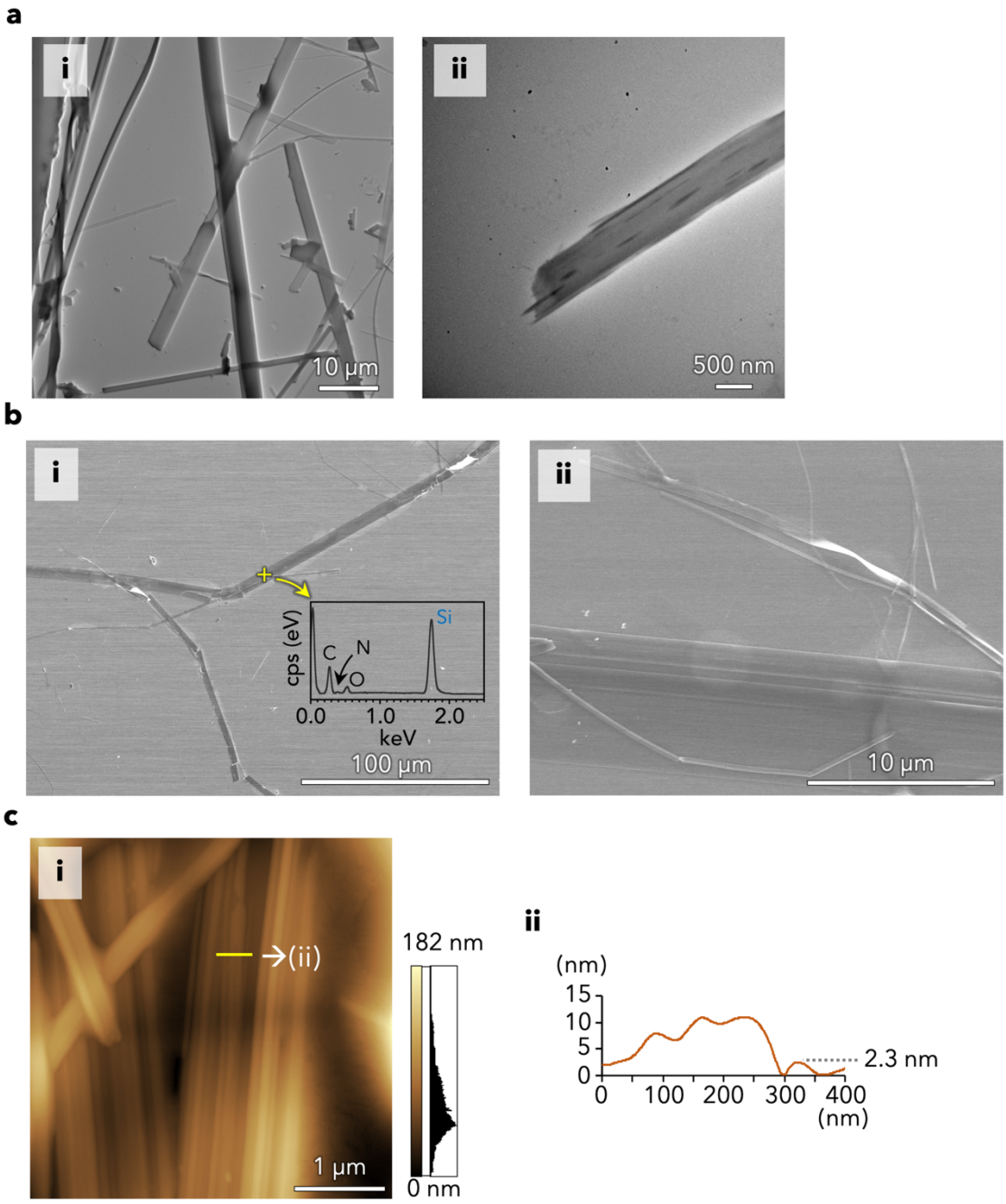

Fig. 3 Microscopic observations of the glyco-microfibers consisting of cellobiose(oNB$_2$)-pNB. a Representative (**i**, **ii**) TEM images of the microfibers on an elastic-carbon-coated grid. **b** Representative (**i**, **ii**) SEM images of the microfibers on a silicon wafer and the corresponding energy-dispersive X-ray spectroscopy (EDS) pattern (inset in **i**) recorded from the yellow mark in the image (**i**). **c** Representative (**i**) AFM height image (tapping mode) of the microfibers on freshly cleaved mica and (**ii**) the corresponding cross-sectional profile along the yellow line in the image (**i**).

To obtain insights into the atomic-scale self-assembly mode, X-ray structural analyses were performed. To our delight, we obtained thin-needle single crystals from 2-propanol, although the crystals were too thin to obtain complete data. Nevertheless, the analyzed crystal structures of cellobiose(oNB_2)-pNB provided valuable insights into the individual molecular conformation as well as the self-assembled structure. First, the X-ray structure of cellobiose(oNB_2)-pNB (**Figs. 4**, **5**) was compared with those of cello-oligosaccharides (such as cellobiose [27]) and cellulose polymorphs (I_α [28], I_β [29], II [30], III_I [31,32]), whose typical structural features are summarized in **Table 1**. In the cellulose polymorphs, the cellulose main chain aligns with the long axis of the fibrils, whereas the packing direction ("parallel" or "antiparallel") is dependent on the polymorphs. That is, parallel packing was observed for triclinic cellulose I_α and monoclinic celluloses I_β and III_I, whereas antiparallel packing was observed for monoclinic cellulose II. In addition, celluloses II and III_I showed "eclipsed" chain packing, whereas the others showed quarter "staggered" chain packing (**Fig. 5d**). Accordingly, the parallel and eclipsed packing modes of the cellobiose(oNB_2)-pNB chains along the *a*-axis disclosed in this study (**Fig. 4a**) are comparable to those of cellulose III_I. Furthermore, the molecular conformations of the cellobiose scaffolds (in which pyranose rings appear in $^4C_1$ conformation) constituting cellobiose(oNB_2)-pNB and cellulose III_I show considerable similarity, as displayed in **Fig. 5b**. For instance, the glycosidic torsion angles [ϕ (O5–C1–O–C4′) and ψ (C1–O–C4′–C3′), see **Table 1** and **Fig. 5a** for definitions] of cellobiose(oNB_2)-pNB are highly similar to those of cellulose III_I and dissimilar to those of cellobiose, which is rather unexpected. In general, ϕ is largely influenced by the *exo*-anomeric effect, whereas ψ is dependent on the noncovalent bonding interactions with nearby residues and solvents [33]. In addition, the orientation of the C6–O6 bonds (**Fig. 5b**), which could be dependent on the hydrogen bonding network patterns of the cellulose polymorphs [28–32] and the gauche effect against the equatorial C4–O4 bond [33], was *gt* (*gauche-trans*) for both cellobiose(oNB_2)-pNB and cellulose III_I (**Fig. 5c**). Overall, we found an unexpected and intriguing similarity between the cellobiose skeletons of cellobiose(oNB_2)-pNB and cellulose III_I, implying that the cellobiose skeleton of cellobiose(oNB_2)-pNB in the self-assembled structures may adopt a thermodynamically stable state, similar to that of cellulose III_I.

Second, the cellobiose(oNB_2)-pNB microfibers obtained by thermal annealing under aqueous conditions (0.10 wt%, 5 °C/min, in Milli-Q water) were also subjected to powder X-ray diffraction (PXRD) analyses. As shown in **Fig. 4b**, there are reasonably overlapped peaks between the obtained PXRD (**Fig. 4b_i**) and the simulated patterns (**Fig. 4b_ii**) for the single-crystal data of cellobiose(oNB_2)-pNB. In addition, the orientation of the needle-like crystal axis indicates that the fiber main axis of the cellobiose(oNB_2)-pNB microfibers is parallel to the *a*-axis (Supplementary **Fig. S3**). Such a molecular arrangement in the fibrous structure is reminiscent of amyloid peptide fibers/fibrils having a cross-β-amyloid structure [4,34]. Hereinafter, we thus refer to this self-assembled architecture of cellobiose(oNB_2)-pNB microfibers as the cross-β-glucan

structure. Notably, the self-assembled (fibrous) architectures of cellobiose [27] and cello-oligosaccharides [11,13] reported previously also have the cross-β-glucan structure. Nonetheless, antiparallel packing (cellulose II type) is frequently observed in the self-assembly structures as far as without additional controlling factors, such as the introduction of alkyl groups at the reducing end of cello-oligosaccharides [35].

Third, there are intriguing differences between the present self-assembled fibrous structure of cellobiose(oNB_2)-pNB and that of a closely related disaccharide (gentiobiose: β-1,6-linked glucose, not β-1,4-linked) derivative bearing aromatic groups, which has recently been reported by another research group [7,8]. In particular, the mode of π interactions among the aromatic groups introduced into the disaccharide scaffolds is significantly different. That is, the crystal structure of cellobiose(oNB_2)-pNB shows offset parallel π–π stacking modes among aromatic rings (oNB and pNB), whereas the C–H···π type edge-to-face interaction mode was unveiled in the self-assembled structure of gentiobiose bearing aromatic groups [7,8]. As described in the molecular design section, the nitro group substituted at the phenyl ring could allow for enhanced π–π interactions, affording offset parallel π–π stacking modes [17-20]. In contrast, according to a Hunter–Sanders model [36] (whose limitation has been actively discussed [21]), an electric quadrupole would play a crucial role in the phenyl ring without a nitro group, resulting in C–H···π type edge-to-face interactions. Although further investigation is required, it is clear that the presence or absence of a nitro group may, at least in part, account for the difference in the self-assembly mode between cellobiose(oNB_2)-pNB bearing nitrophenyl groups and gentiobiose bearing pristine phenyl rings. The center-of-mass distance between the stacked NB rings was estimated to be 4.5 Å ("distances to rings" tool implemented in PyMOL was used) for the offset parallel π–π stacking, as displayed in **Fig. 4a**. This distance is almost comparable to previously reported distances for the "center-to-center spacing" of aromatic rings [17,21]. Interestingly, the offset parallel π–π stacking distance coincided with the face-to-face stacking distances of the glucose rings in the cellobiose scaffold (4.5 Å) [27] and that of cellulose III_I (4.4 Å) [31]. These complementary distances may be crucial for the formation of the thermodynamically stable 1D self-assembled architecture of cellobiose(oNB_2)-pNB microfibers having the cross-β-glucan structure.

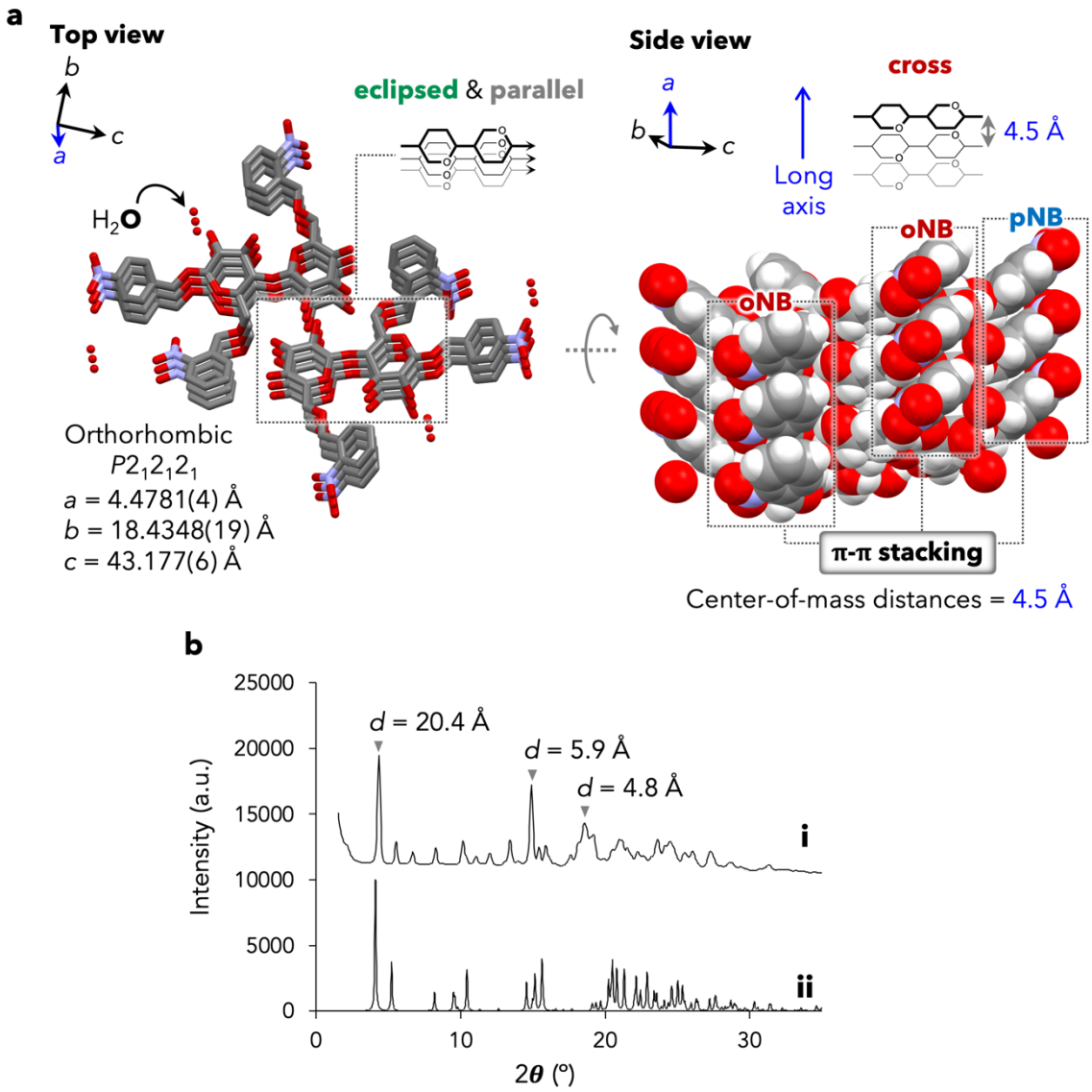

Fig. 4 Structural analysis of the glyco-microfibers consisting of cellobiose(oNB$_2$)-pNB. a X-ray structures (gray: carbon, red: oxygen, blue: nitrogen, white: hydrogen. Top view: stick model; all hydrogens are omitted for clarity. Side view: space-filling model; oxygen atoms of water molecules are presented) of single-crystal [cellobiose(oNB$_2$)-pNB·H$_2$O] obtained from 2-propanol (Supplementary **Fig. S3**, for long axis of the needle-like crystal). **b** (**i**) Experimental PXRD pattern of cellobiose(oNB$_2$)-pNB microfibers (three representative peaks are picked up as *d*-spacing) and (**ii**) simulated pattern for the needle-like single-crystal data of cellobiose(oNB$_2$)-pNB.

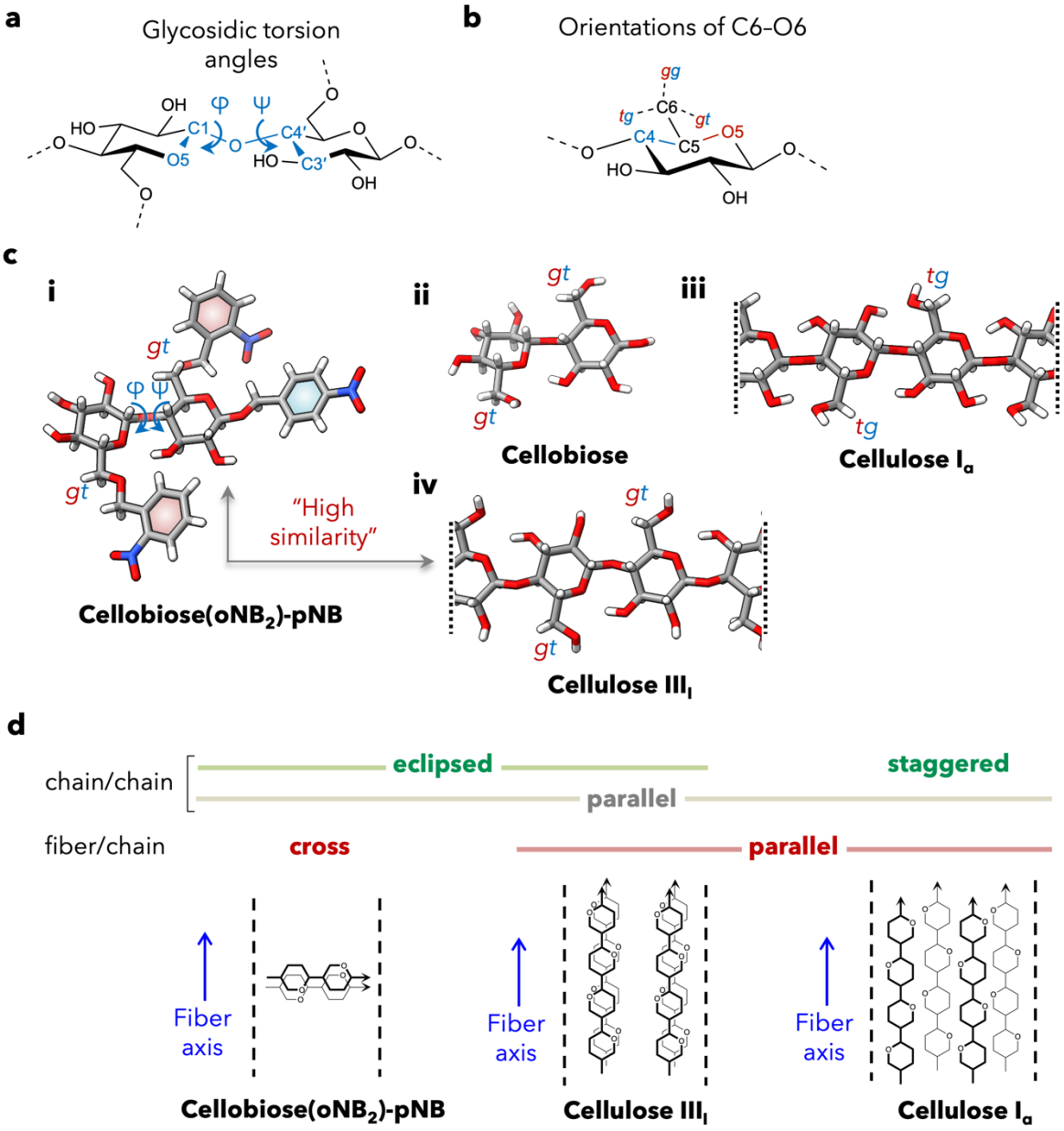

Fig. 5 Structural parameters of the cellobiose-based compounds. a Glycosidic torsion angles defined by the International Union of Pure and Applied Chemistry (IUPAC) convention [37] or the C–1 crystallographic style [38]: ϕ (O5–C1–O–C4′) and ψ (C1–O–C4′–C3′)] for the cellobiose unit (β1→4-linked). **b** Orientation of the C6–O6 bond (*tg*, *gg*, *gt*: *t* and *g* denote *trans* and *gauche* conformations, respectively) for the β-glucose unit. The first *g* or *t* refers to the position of O6 against O5 (O5–C5–C6–O6), whereas the second *g* or *t* refers to the position of O6 against C4 (C4–C5–C6–O6). **c** Glycosidic torsion angles and orientation of the C6–O6 bond of (**i**) cellobiose(oNB$_2$)-pNB, (**ii**) β-cellobiose, (**iii**) cellulose I$_\alpha$, and (**iv**) cellulose III$_\text{I}$. There is a rather high similarity between those of (**i**) cellobiose(oNB$_2$)-pNB and (**iv**) cellulose III$_\text{I}$ (see also **Table 1**). **d** Schematic representations of the packing manners of the main chains and their orientations against or along the fiber main

axis.

Table 1. Glycosidic torsion angles (degrees) [C–1 crystallographic style: ϕ (O5–C1–O–C4′) and ψ (C1–O–C4′–C3′)] and the orientation of the C6–O6 bond (*tg*, *gg*, *gt*) for the cellobiose units of cellobiose(oNB$_2$)-pNB, β-cellobiose, and cellulose polymorphs (I_α, I_β, II, III_I) (see also **Figs. 5a**,**b** for the definitions) and packing arrangement of the cellobiose or cellulose main chains.

Compounds	Glycosidic torsion angles (degrees)		Orientation of the C6–O6 bonds	Packing arrangement of the cellobiose or cellulose main chains
	ϕ	ψ		
Cellobiose(oNB$_2$)-pNB	–90.1	91.6	*gt*	parallel
β-Cellobiose[a]	–75.7	106.5	*gt*	parallel
Cellulose I_α[b]	–97.7	99.2	*tg*	parallel
Cellulose I_β[c]	–98.4	90.5	*tg*	parallel
Cellulose II[d]	–96.8	95.0	*gt*	antiparallel
Cellulose III_I[e]	–91.9	93.0	*gt*	parallel

[a]β-Cellobiose: (CCDC 1920084) [27], [b]Cellulose I_α: [28], [c]Cellulose I_β: [29], [d]Cellulose II: [30], [e]Cellulose III_I: [31]. All cif files for the cellulose polymorphs (Cellulose I_α, I_β, II, and III_I) were obtained from a previous study [32].

Photo-responsiveness of the cellobiose(oNB$_2$)-pNB microfibers. Finally, we evaluated the photo-responsiveness of the cellobiose(oNB$_2$)-pNB microfibers [typical preparation conditions; 0.10 wt% (1.3 mM), 20 °C/min, in 100 mM HEPES-NaOH (pH 7.4) containing 2 vol% DMSO]. The oNB groups introduced at the C6 positions of cellobiose(oNB$_2$)-pNB can be removed by ultraviolet (UV)-light irradiation, as shown in the plausible scheme in **Fig. 6a** [39,40]. Such a photo-induced transformation of the chemical structure should increase the aqueous solubility and result in the disassembly of the cellobiose(oNB$_2$)-pNB microfibers under aqueous conditions. For instance, pristine cellobiose exhibits low, but reasonable solubility in water at concentrations of 39.4 mM [41] or 14 g/100 g [42], well above the typical concentration of cellobiose(oNB$_2$)-pNB (0.10 wt%, 1.3 mM) at which microfibers are formed. As expected, upon irradiation with UV light (365 nm, LED), the cellobiose(oNB$_2$)-pNB microfibers were degraded within 3 min, as shown in **Fig. 6b_i**. Notably, a non-negligible amount of brown precipitates remained, probably owing to the formation of aqueous insoluble residues derived from the photo-removed 2-nitrobenzyl groups (e.g., 2-nitrosobenzaldehyde)

[39]. Nonetheless, encouraged by this result, a film mask rendering a 20 μm width line was set in front of the UV light source. As displayed in **Fig. 6b_ii**, the spatio-controlled degradation of the cellobiose(oNB_2)-pNB microfibers was demonstrated, which is one of the advantages of photo-responsiveness [39]. To evaluate the molecular transformation induced by the UV-light irradiation, ^{1}H NMR spectroscopic analyses were performed after dissolving the lyophilized samples in a solution of DMSO-d_6:D_2O = 5:1 (*v*/*v*). Cellobiose(oNB_2)-pNB (**Fig. 6c_i**) and cellobiose (**Fig. 6c_iv**) molecules can be dissolved in this mixed solution. After UV-light irradiation to complete the degradation of the cellobiose(oNB_2)-pNB microfibers (Supplementary **Fig. S4**), the number of peaks assignable to the oNB groups (peaks: "b,c,d,f,h") decreased significantly, whereas those for the pNB group (peaks: "a,e,g,i") remained almost unchanged, as shown in **Fig. 6c_ii**. Furthermore, by membrane filtration (pore size: 0.45 μm) to remove precipitates before lyophilization, the obtained spectrum (**Fig. 6c_iii**) can almost be exclusively assigned to cellobiose-pNB, as displayed in **Fig. 6a**. Collectively, these results indicate that the two oNB groups introduced into cellobiose(oNB_2)-pNB were selectively removed by UV-light irradiation, inducing the disassembly of the cellobiose(oNB_2)-pNB microfibers.

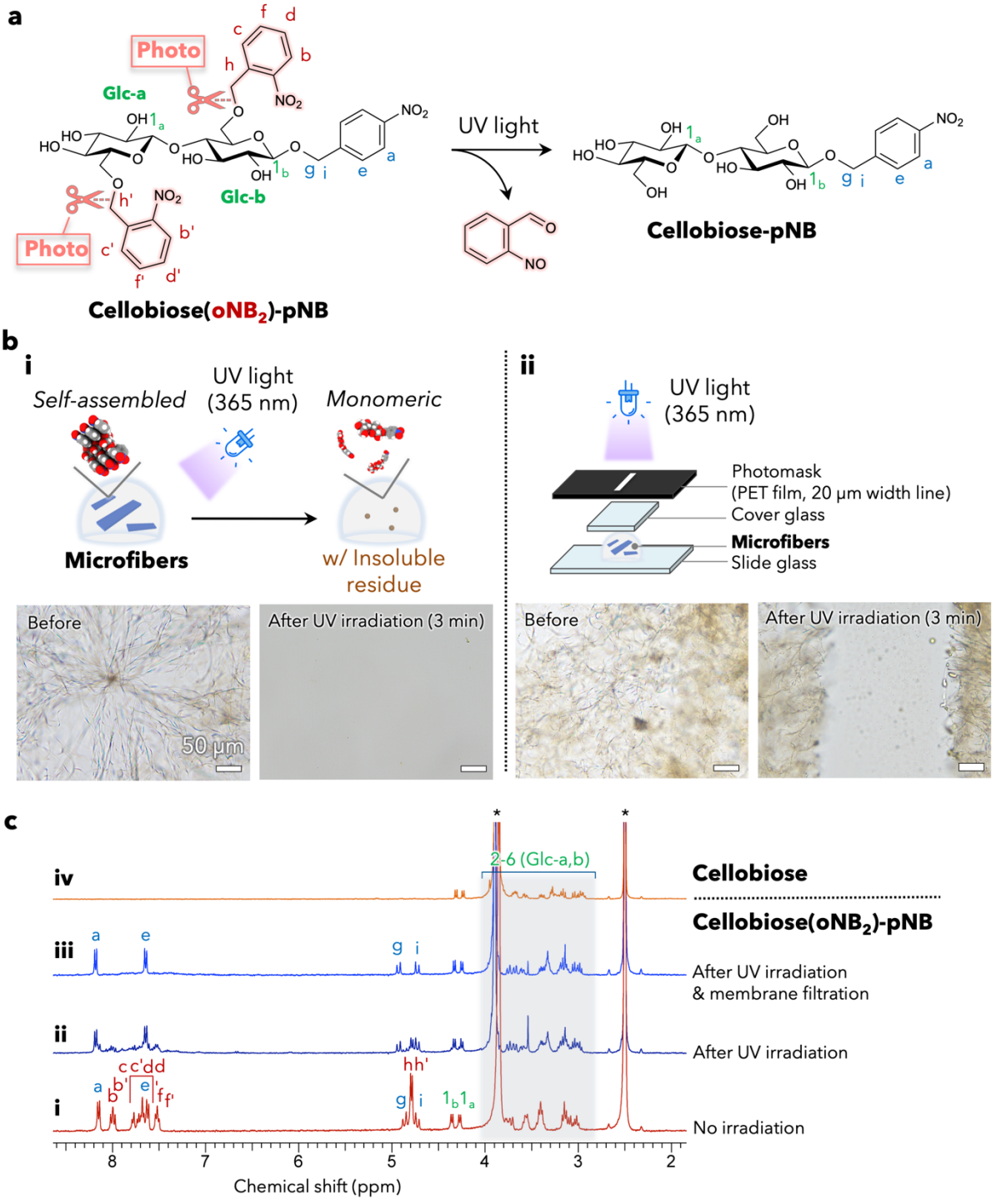

Fig. 6 Photo-responsiveness of the cellobiose(oNB$_2$)-pNB microfibers. a Plausible photo-responsive transformation of cellobiose(oNB$_2$)-pNB to afford a potentially water-soluble compound (i.e., cellobiose-pNB). **b** Representative OM images before and after UV-light irradiation (LED, 365 nm) (**i**) with or (**ii**) without a photomask. Scale bar: 50 μm. **c** ^{1}H NMR spectra [400 MHz, DMSO-d_6:D$_2$O = 5:1 (*v*/*v*)] of the samples prepared from the cellobiose(oNB$_2$)-pNB microfibers (**i**) before and (**ii**, **iii**) after UV-light irradiation (**ii**) with or

(**iii**) without membrane filtration before lyophilization and (**iv**) cellobiose (see Supplementary **Fig. S4** for the experimental protocols to prepare the samples).

Conclusion

We successfully constructed photodegradable glyco-microfibers from self-assembling, discrete cellobiose derivatives bearing a nitrobenzyl group, using a semi-rational molecular design and a robust but flexible chemical synthesis procedure. The supramolecular architecture of the self-assembled cellobiose derivative at the atomic level was revealed and compared with those reported previously for pristine cellobiose and cellulose polymorphs. Such structural elucidation unveiling a 1D self-assembled architecture (cross-β-glucan structure) would offer valuable insights for the rational, future molecular design of glyco-materials based on not only cellobiose but also cello-oligosaccharide scaffolds. We believe that stimuli-responsive glyco-microfibers, such as those developed in this study, may provide a unique opportunity to explore various (bio)applications.

Methods

Preparation of the cellobiose(oNB$_2$)-pNB microfibers. Typically, a DMSO solution (50 mg/mL, 2.0 μL) of cellobiose(oNB$_2$)-pNB and an aqueous buffer [100 mM HEPES-NaOH (pH 7.4), 98 μL] was mixed in a 0.2-mL PCR tube. Thereafter, the sample was subjected to thermal treatment [heated at 95 °C for 5 min, followed by slowly cooling to 25 °C at the designated rate (5, 10, and 30 °C/min)] with a thermal cycler (T100, Bio-Rad) or a dry bath incubator (Mini Cooler, Major Science).

OM and POM observations. The suspension prepared, as described above, was dropped on a micro slide glass (size: 76 × 26 mm, thickness: 0.8–1.0 mm, Matsunami) and covered with a glass coverslip (size: 18 × 18 mm, thickness: 0.13–0.17 mm, Matsunami). The specimen was observed using a polarized optical microscope (BX53LED, Olympus) equipped with a CMOS camera (AdvanCam-U3, AdvanVision). The OM and POM (under cross-polarizer) images were obtained and analyzed using the AdvanView acquisition software equipped with a camera. UPLFLN series objectives (4×, 10×, 20×, and 40×) were employed for the observations.

TEM observations. The sample (approx. 10 μL) was dropped on a copper TEM grid covered by an elastic carbon-support film (20–25 nm), and the excess solution was immediately blotted with filter paper. The TEM grid was dried under reduced pressure for at least 6 h before TEM observation without staining. TEM images were acquired using a Hitachi H7000 (accelerating voltage: 100 kV) equipped with a CCD camera and analyzed with ImageJ on a Windows PC.

SEM observations. The sample (approx. 10 μL) was dropped on a silicon wafer, and the excess solution was immediately blotted with filter paper. The specimen was dried under reduced pressure for at least 6 h before SEM observation. SEM images were acquired using a Hitachi S-4800 (accelerating voltage: 15 kV) equipped with an Oxford Instruments Ultim Max 100 detector for EDS analysis (Aztec software, Oxford instruments). Osmium coating (10 s) was performed using Neoc-Pro/p (Meiwafosis Co., Ltd.) for specimens containing the cellobiose(oNB_2)-pNB microfibers.

AFM observations. The sample (approx. 10 μL) was dropped on freshly cleaved mica, and the excess solution was removed by blotting with a filter paper. The AFM observations (512 × 512 px resolution) were performed using a Shimadzu SPM-9700HT microscope in air at ambient temperature, with standard silicon cantilevers (AR5-NCHR, Nanosensors) in tapping mode.

Single-crystal X-ray diffraction analysis of cellobiose(oNB_2)-pNB. A single crystal (size: 0.08 × 0.03 × 0.01 mm^3) of cellobiose(oNB_2)-pNB·H_2O ($C_{33}H_{37}N_3O_{17}·H_2O$, M_w = 765.67) suitable for X-ray analysis was grown by the recrystallization of a solution of cellobiose(oNB_2)-pNB in 2-propanol at ambient temperature. XRD data were collected using an XtaLAB AFC10 diffractometer equipped with a HyPix-6000HE hybrid pixel array detector with Mo $K\alpha$ radiation (λ = 0.71073 Å) at 150 K (Cambridge Crystallographic Centre by referencing CCDC number 2310825). In addition, the orientation of the crystal axis was determined by single-crystal X-ray diffraction using CrysAlisPro software [43].

Powder X-ray diffraction of the cellobiose(oNB_2)-pNB microfibers. PXRD analysis using Cu $K\alpha$ radiation (λ = 1.54178 Å) (45 kV, 45 mA) was performed on cellobiose(oNB_2)-pNB microfibers filled inside a glass capillary (outside ϕ = 1.0 mm) using a Rigaku R-AXIS IV X-ray diffractometer. The diffracted radiation was recorded using an imaging plate with a sample-to-detector distance of 165 mm and an exposure time of 30 min. DMSO, which is useful in the preparation of aqueous solutions under the various conditions discussed above, and the buffering component were not employed in the preparation of the samples for PXRD to circumvent potential interference from them. Nevertheless, their influence on the formation of microfibers was not significant, at least according to the OM images.

Photoirradiation. An aqueous dispersion containing cellobiose(oNB_2)-pNB microfibers was dropped on a micro slide glass (size: 76 × 26 mm, thickness: 0.8–1.0 mm, Matsunami) and covered with a glass coverslip (size: 18 × 18 mm, thickness: 0.13–0.17 mm, Matsunami) to enable the use of a photomask obtained from

MEMSFILM.com (Japan). A UV LED source [PER-AMP, PER-365 (365 nm at 360 mW), 350 mA, Techno Sigma (Japan)] was used for the photoirradiation.

Data availability

All other data are available from the corresponding author on reasonable request. The X-ray crystallographic coordinate for cellobiose(oNB_2)-pNB has been deposited at the CCDC, under deposition number 2310825. These data can be obtained free of charge from The Cambridge Crystallographic Data Centre via www.ccdc.cam.ac.uk.

References

1. Wilson, C. J., Bommarius, A. S., Champion, J. A., Chernoff, Y. O., Lynn, D. G., Paravastu, A. K., Liang, C., Hsieh, M. C., & Heemstra, J. M. Biomolecular assemblies: moving from observation to predictive design. *Chem. Rev.* **118**, 11519–11574 (2018).
2. Du, X., Zhou, J., & Xu, B. Supramolecular hydrogels made of basic biological building blocks. *Chem. Asian J.* **9**, 1446–1472 (2014).
3. Schmid, S. Y., Lachowski, K., Chiang, H. T., Pozzo, L., De Yoreo, J., & Zhang, S. Mechanisms of biomolecular self-assembly investigated through in situ observations of structures and dynamics. *Angew. Chem. Int. Ed.* **62**, e202309725 (2023).
4. Ke, P. C., Zhou, R., Serpell, L. C., Riek, R., Knowles, T. P. J., Lashuel, H. A., Gazit, E., Hamley, I. W., Davis, T. P., Fändrich, M., Otzen, D. E., Chapman, M. R., Dobson, C. M., Eisenberg, D. S., & Mezzenga, R. Half a century of amyloids: past, present and future. *Chem. Soc. Rev.* **49**, 5473–5509 (2020).
5. Panja, S., & Adams, D. J. Stimuli responsive dynamic transformations in supramolecular gels. *Chem. Soc. Rev.* **50**, 5165–5200 (2021).
6. Ramakrishnan, M., van Teijlingen, A., Tuttle, T., & Ulijn, R. V. Integrating computation, experiment, and machine learning in the design of peptide-based supramolecular materials and systems. *Angew. Chem. Int. Ed.* **62**, e202218067 (2023).
7. Yu, Y., Gim, S., Kim, D., Arnon, Z. A., Gazit, E., Seeberger, P. H., & Delbianco, M. Oligosaccharides self-assemble and show intrinsic optical properties. *J. Am. Chem. Soc.* **141**, 4833–4838 (2019).
8. Gim, S., Fittolani, G., Nishiyama, Y., Seeberger, P. H., Ogawa, Y., & Delbianco, M. Supramolecular assembly and chirality of synthetic carbohydrate materials. *Angew. Chem. Int. Ed.* **59**, 22577–22583 (2020).
9. Li, T., Chen, C., Brozena, A. H., Zhu, J. Y., Xu, L., Driemeier, C., Dai, J., Rojas, O. J., Isogai, A., Wågberg,

L., & Hu, L. Developing fibrillated cellulose as a sustainable technological material. *Nature* **590**, 47–56 (2021).

10. Etale, A., Onyianta, A. J., Turner, S. R., & Eichhorn, S. J. Cellulose: A review of water interactions, applications in composites, and water treatment. *Chem. Rev.* **123**, 2016–2048 (2023).
11. Sakurai, Y., Sawada, T. & Serizawa, T. Phosphorylase-catalyzed synthesis and self-assembled structures of cellulose oligomers in the presence of protein denaturants. *Polym. J.* **54**, 561–569 (2022).
12. Zhong, C. & Nidetzky, B. Precision synthesis of reducing-end thiol-modified cellulose enabled by enzyme selection. *Polym. J.* **54**, 551–560 (2022).
13. Fittolani, G., Vargová, D., Seeberger, P. H., Ogawa, Y., & Delbianco, M. Bottom-up approach to understand chirality transfer across scales in cellulose assemblies. *J. Am. Chem. Soc.* **144**, 12469–12475 (2022).
14. Higashi, S. L., Shintani, Y., & Ikeda, M. Installing reduction responsiveness into biomolecules by introducing nitroaryl groups. *Chem. –Eur. J.* **28**, e202201103 (2022).
15. Shieh, P., Hill, M. R., Zhang, W., Kristufek, S. L., & Johnson, J. A. Clip chemistry: diverse (bio)(macro)molecular and material function through breaking covalent bonds. *Chem. Rev.* **121**, 7059–7121 (2021).
16. Wang, J., Wang, X., Fan, X., & Chen, P. R. Unleashing the power of bond cleavage chemistry in living systems. *ACS Cent. Sci.* **7**, 929–943 (2021).
17. Liyanage, W., Brennessel, W., & Nilsson, B. Spontaneous transition of self-assembled hydrogel fibrils into crystalline microtubes enables a rational strategy to stabilize the hydrogel state. *Langmuir* **31**, 9933–9942 (2015).
18. Liyanage, W. & Nilsson, B. L. Substituent effects on the self-assembly/coassembly and hydrogelation of phenylalanine derivatives. *Langmuir* **32**, 787–799 (2016).
19. Ohtomi, T., Higashi, S. L., Mori, D., Shibata, A., Kitamura, Y., & Ikeda, M. Effect of side chain phenyl group on the self-assembled morphology of dipeptide hydrazides. *Pept. Sci.* **113**, e24200 (2020).
20. Rashkin, M. J., & Waters, M. L. Unexpected substituent effects in offset pi-pi stacked interactions in water. *J. Am. Chem. Soc.* **124**, 1860–1861 (2002).
21. Carter-Fenk, K., Liu, M., Pujal, L., Loipersberger, M., Tsanai, M., Vernon, R. M., Forman-Kay, J. D., Head-Gordon, M., Heidar-Zadeh, F., & Head-Gordon, T. The energetic origins of pi-pi contacts in proteins. *J. Am. Chem. Soc.* **145**, 24836–24851 (2023).
22. Yuan, C., Levin, A., Chen, W., Xing, R., Zou, Q., Herling, T. W., Challa, P. K., Knowles, T. P. J., & Yan, X. Nucleation and growth of amino acid and peptide supramolecular polymers through liquid-liquid phase separation. *Angew. Chem. Int. Ed.* **58**, 18116–18123 (2019).

23. Shen, Y., Ruggeri, F. S., Vigolo, D., Kamada, A., Qamar, S., Levin, A., Iserman, C., Alberti, S., George-Hyslop, P. S., & Knowles, T. P. J. Biomolecular condensates undergo a generic shear-mediated liquid-to-solid transition. *Nat. Nanotechnol.* **15**, 841–847 (2020).
24. Gregory, K. P., Elliott, G. R., Robertson, H., Kumar, A., Wanless, E. J., Webber, G. B., Craig, V. S. J., Andersson, G. G., & Page, A. J. Understanding specific ion effects and the Hofmeister series. *Phys. Chem. Chem. Phys.* **24**, 12682–12718 (2022).
25. Wei W. Hofmeister effects shine in nanoscience. *Adv. Sci.* **10**, e2302057 (2023).
26. Knowles, T. P., Vendruscolo, M., & Dobson, C. M. The amyloid state and its association with protein misfolding diseases. *Nat. Rev. Mol. Cell Biol.* **15**, 384–396 (2014).
27. Yimin Mao, Y. & Zavalij, P. Y. *CSD Communication*, CCDC 1920084: DOI: 10.5517/ccdc.csd.cc22g06s (2019).
28. Nishiyama, Y., Sugiyama, J., Chanzy, H., & Langan, P. Crystal structure and hydrogen bonding system in cellulose I_α from synchrotron X-ray and neutron fiber diffraction. *J. Am. Chem. Soc.* **125**, 14300–14306 (2003).
29. Nishiyama, Y., Langan, P., & Chanzy, H. Crystal structure and hydrogen-bonding system in cellulose I_β from synchrotron X-ray and neutron fiber diffraction. *J. Am. Chem. Soc.* **124**, 9074–9082 (2002).
30. Langan, P., Nishiyama, Y., & Chanzy, H. X-ray structure of mercerized cellulose II at 1 Å resolution. *Biomacromolecules* **2**, 410–416 (2001).
31. Wada, M., Chanzy, H., Nishiyama, Y., & Langan, P. Cellulose III_I crystal structure and hydrogen bonding by synchrotron x-ray and neutron fiber diffraction. *Macromolecules* **37**, 8548–8555 (2004).
32. French, A. D. Idealized powder diffraction patterns for cellulose polymorphs. *Cellulose* **21**, 885–896 (2014).
33. Wormald, M. R., Petrescu, A. J., Pao, Y. L., Glithero, A., Elliott, T., & Dwek, R. A. Conformational studies of oligosaccharides and glycopeptides: complementarity of NMR, X-ray crystallography, and molecular modelling. *Chem. Rev.* **102**, 371–386 (2002).
34. Eisenberg, D. & Jucker, M. The amyloid state of proteins in human diseases. *Cell* **148**, 1188–1203 (2012).
35. Yataka, Y., Sawada, T., & Serizawa, T. Multidimensional self-assembled structures of alkylated cellulose oligomers synthesized via in vitro enzymatic reactions. *Langmuir* **32**, 10120–10125 (2016).
36. Hunter, C. A. & Sanders, J. K. M. The nature of π-π interactions. *J. Am. Chem. Soc.* **112**, 5525–5534 (1990).
37. IUPAC-IUB Joint Commission on Biochemical Nomenclature, *Pure Appl. Chem.* **55**, 1269–1272 (1983).
38. Lütteke, T. Analysis and validation of carbohydrate three-dimensional structures. *Acta Cryst.* **65**, 156–168 (2009).

39. Zehavi, U., Amit, B., & Patchornik, A. Light-sensitive glycosides. I. 6-Nitroveratryl β-D-glucopyranoside and 2-nitrobenzyl β-D-glucopyranoside. *J. Org. Chem.* **37**, 2281–2285 (1972).
40. Klán, P., Šolomek, T., Bochet, C. G., Blanc, A., Givens, R., Rubina, M., Popik, V., Kostikov, A., & Wirz, J. Photoremovable protecting groups in chemistry and biology: reaction mechanisms and efficacy. *Chem. Rev.* **113**, 119–191 (2013).
41. Liu, Z., Zhang, C., Liu, R., Zhang, W., Kang, H., Li, P., & Huang, Y. Dissolution of cellobiose in the aqueous solutions of chloride salts: Hofmeister series consideration. *Cellulose* **23**, 295–305 (2016).
42. Jónsdóttir, S. O., Cooke, S. A., & Macedo, E. A. Modeling and measurements of solid-liquid and vapor-liquid equilibria of polyols and carbohydrates in aqueous solution. *Carbohydrate Res.* **337**, 1563–1571 (2002).
43. CrysAlisPro CCD, CrysAlisPro RED and ABSPACK in CrysAlisPro RED; Oxford Diffraction Ltd.: Abingdon, England, 2006.

Acknowledgments

This work was supported in part by financial supports by JSPS KAKENHI grant (grant number: 23H01815, M.I. N.K.), iGCORE collaborating grant, JSPS Core-to-Core program (grant number: JPJSCCA20200007, H.A.), and JST CREST (grant number: JPMJCR18H2, H.A.) and from the Takeda Science Foundation. We acknowledge Life Science Research Center and Research Equipment Sharing Promotion Center, Gifu University for the maintenance of the instruments and their kind support. Finally, the authors thank Enago (www.enago.jp) for the English language review.

Author contributions

B. O.: formal analysis, investigation, methodology, validation, visualization, and writing–original draft; E. Y.: formal analysis, investigation, methodology, resources, and validation; N. K.: conceptualization, formal analysis, funding acquisition, investigation, methodology, supervision, validation, visualization, writing–review & editing; T. O.: formal analysis, investigation, methodology, and validation; S.-i. K.: formal analysis, investigation, methodology, and validation; H. K.: formal analysis, investigation, methodology, and validation; H. A.: conceptualization, funding acquisition, methodology, project administration, supervision, validation, writing–review & editing; M. I.: conceptualization, formal analysis, funding acquisition, investigation, methodology, supervision, validation, visualization, writing; All authors have given approval to the final version of the manuscript.

Competing interests

The authors declare no competing interests.

Additional information

Supplementary information The online version contains supplementary material available.

Correspondence and requests for materials should be addressed to Naoko Komura, Hiromune Ando and Masato Ikeda